2019

Chemically dealloyed Fe-based metallic glass with void channels-like architecture for highly enhanced peroxymonosulfate activation in catalysis

J.C. Wang
Edith Cowan University

S.X. Liang
Edith Cowan University

Z. Jia

W.C. Zhang

W.M. Wang

See next page for additional authors

Authors

J.C. Wang, S.X. Liang, Z. Jia, W.C. Zhang, W.M. Wang, Y.J. Lui, J. Lu, and L.C Zhang

Accepted Manuscript

Chemically dealloyed Fe-based metallic glass with void channels-like architecture for highly enhanced peroxymonosulfate activation in catalysis

J.C. Wang, S.X. Liang, Z. Jia, W.C. Zhang, W.M. Wang, Y.J. Liu, J. Lu, L.C. Zhang

Please cite this article as: J.C. Wang, S.X. Liang, Z. Jia, W.C. Zhang, W.M. Wang, Y.J. Liu, J. Lu, L.C. Zhang, Chemically dealloyed Fe-based metallic glass with void channels-like architecture for highly enhanced peroxymonosulfate activation in catalysis, *Journal of Alloys and Compounds* (2019), doi: https://doi.org/10.1016/j.jallcom.2019.01.130.

Chemically dealloyed Fe-based metallic glass with void channels-like architecture for highly enhanced peroxymonosulfate activation in catalysis

J.C. Wang [a], S.X. Liang [a], Z. Jia[b,c*], W.C. Zhang[d], W.M. Wang[e], Y.J. Liu[a], J. Lu[b,c,f], L.C. Zhang[a,*]

[a]School of Engineering, Edith Cowan University, 270 Joondalup Drive, Joondalup, Perth, WA 6027, Australia

[b]Hong Kong Branch of National Precious Metals Material Engineering Research Center, Department of Material Science and Engineering, City University of Hong Kong, Hong Kong, China

[c]Department of Mechanical Engineering, City University of Hong Kong, Hong Kong, China

[d]Environmental Protection Administration of Ji'an City, Ji'an, Jiangxi Province, 343000, China

[e]School of Materials Science and Engineering, Shandong University, Jinan, Shandong Province, 250061, China

[f]Centre for Advanced Structural Materials, City University of Hong Kong, Shenzhen Research Institute, 8 Yuexing 1st Road, Shenzhen Hi-Tech Industrial Park, Nanshan District, Shenzhen, Guangdong Province, 518000, China

Abstract

Metallic glasses (MGs) with their intrinsic disordered atomic structure and widely controllable atomic components have recently emerged as fascinating functional materials in wastewater treatment. Compared to crystalline alloys, the less-noble atomic components in monolithic metallic glass are more efficient to be selectively dissolved during dealloying process. This work reported a facile chemical dealloying approach to fabricate a void channels-like structured MG with the elemental components of $Fe_{73.5}Si_{13.5}B_9Cu_1Nb_3$ for methylene blue (MB) degradation. Results indicated that the dealloyed $Fe_{73.5}Si_{13.5}B_9Cu_1Nb_3$ MGs with the void channels-like morphology presented a significant improvement of catalytic efficiency and reusability. The dye degradation reaction rate (k_{obs}) of the dealloyed $Fe_{73.5}Si_{13.5}B_9Cu_1Nb_3$ MGs presented 3 times higher than their as-spun MGs. More importantly, the dealloyed $Fe_{73.5}Si_{13.5}B_9Cu_1Nb_3$ MGs can be reused up to 25 times without significantly loosing catalytic efficiency. It was also found that the dealloyed $Fe_{73.5}Si_{13.5}B_9Cu_1Nb_3$ MGs exhibited a greater corrosion resistance in the simulated dye solution compared to the as-spun ribbons, demonstrating a robust self-healing ability in catalytic activity. This work provides a novel view for designing MG catalysts with high efficiency and stability in worldwide energy and environmental concerns.

Keywords: Metallic glass; Amorphous; Surface roughness; Stability; Heterogeneous catalysis

---

*Corresponding authors: zhejia@cityu.edu.hk (Z.J.); l.zhang@ecu.edu.au, lczhangimr@gmail.com (L.C.Z.)

1. Introduction

Metallic glasses (MGs), also alternatively named as amorphous alloys, have emerged as great potential catalysts in treating industrial pollutants because of their ultra-fast efficiency, high reusability and environmentally-friendly properties [1-3]. Many reports have demonstrated that the MGs with intrinsically catalytic advantages, such as disordered atomic packing structure [4, 5], high free Gibbs energy [6, 7] and abundant active sites [8, 9], are becoming a new promising and competitive member in the big family of catalysts. Recent studies indicate that the MGs with widely tunable atomic components, such as Fe- [10-24], Mg- [7, 25-30], Al- [31, 32], Co- [33] and Ni-based [34] alloys, indeed have catalytically active and uniquely selectivity in both reductive and oxidative wastewater remediation. For example in the reductive reaction, it is found that the ball-milled (BM) $Fe_{73}Nb_3Si_7B_{17}$ [6] and $Mg_{73}Zn_{21.5}Ca_{5.5}$ [7] MG powders with the high free Gibbs energy and large active sites presented 200 times and 1000 times higher catalytic efficiency than their crystalline counterparts, respectively. The melt-spun $Al_{91-x}Ni_9Y_x$ glassy ribbon could effectively purify direct blue 2B dye in a wide pH conditions, demonstrating extensive application of MGs in the wastewater treatment [32]. The BM $Co_{78}Si_8B_{14}$ MG powder with a large specific surface area exhibited one order and three orders higher magnitudes of essential dye degradation ability than the Co- and Fe-based crystalline powder, respectively [33]. With respect to the advanced oxidation processes (AOPs) [35], MGs present ultrafast activation efficiency for various peroxides including hydrogen peroxides (H_2O_2) [36], persulfate (PS) [37] and peroxymonosulfate (PMS) [38]. For instance, using $Fe_{78}Si_9B_{13}$ and $Fe_{73.5}Si_{13.5}B_9Cu_1Nb_3$ glassy ribbons as catalysts presented 5 - 10 times higher activation efficiency of H_2O_2 than

the currently employed Fe-based crystalline catalysts [11]. The $Fe_{78}Si_9B_{13}$ MGs could rapidly activate H_2O_2, PS and PMS to produce highly reactive radicals towards complete crystal violet dye degradation within 15 min [39] and could be reused up to 20 times when activating PS without significantly loosing catalytic efficiency [37] and so on. Therefore, as a new type of promising catalyst, MGs have been promoted to be the cutting edge of advanced material research and industrial practical applications. However, due to their unique amorphization process (rapid solidification or mechanical alloying), the presented specific surface area of MGs are relatively lower than other porous/nanoporous metallic catalysts. For further facilitating their catalytic activity, the alteration of surface morphology of MGs should be importantly explored to provide more active sites in the theoretical and practical study.

Among all the preparation processes of turning surface morphology, the chemical dealloying has been attracting great attentions due to their facile and cost-effective advantages. The dealloyed catalysts with a large surface roughness and high electrical conductivity present significant enhancement in the catalytic applications [19, 26, 40]. Compared with the traditional crystalline alloys with complex phases, large grain boundaries and few atomic components, the multi-component MGs (i.e. 2-6 components) with a monolithic phase and homogeneous atomic distribution present large interests in enlarging their surface roughness in catalytic application. So far, many attempts have been investigated to optimize the surface morphology using MGs as the precursors by chemical dealloying. For example, it is reported that the porous structured Y-Ni-Co MGs with a large specific surface area could be designed by chemical dealloying of Al from $Al_{85}Y_6Ni_6Co_3$ MGs, presenting a promoted activity in

energy storage [41]. The nanoporous Pd-Cu-S catalysts prepared by chemical dealloying of Ti-Cu-Pd MGs exhibited a highly active catalytic efficiency in hydrogen evolution reaction [42]. A core-shell structure with face-centered-cubic structured Cu enveloped by Mg-based amorphous matrix could be designed by chemical dealloying of Mg-Cu-Y MGs, highly facilitating the degradation efficiency of direct blue 6 dye [26]. The chemically dealloyed nanoporous architecture in Fe-Si-B-P [19] and Fe-Si-B-Nb [40] MGs demonstrated a lower activation energy and larger specific surface area in dye degradation compared to their as-prepared MGs. The alteration of surface morphology obtained by chemical dealloying method provide a vivid portrait into the surface roughness design of novel MG catalysts. Therefore, selecting the atomic components to be dealloyed in MGs remains a great challenge in catalysis.

It is well accepted that the initial consideration of designing the elemental components in MGs is their glass forming ability [43-45]. The proper addition of metalloids, such as Si and B, could remarkably improve their formation of amorphous structure. On this basis, the micro-alloying into MGs may affect their intrinsic atomic structure so as to effectively alter their dealloyed architectures. In addition, a severe crystallization behavior usually occurrs in previously reported MGs during the chemical dealloying [19, 26, 41], which will subsequently affect their catalytic properties more or less. In this work, the fabrication of void channels-like architectures in $Fe_{73.5}Si_{13.5}B_9Cu_1Nb_3$ MGs under different acidic conditions is systermatically discussed to improve their surface roughness for promoting the catalytic performance. The designed MGs are manufactured by a melt-spinning method and their corresponding amorphous nature is characterized. Although the $Fe_{73.5}Si_{13.5}B_9Cu_1Nb_3$

glassy ribbons have been reported as catalysts in treating various industrial pollutants [11], the comparative study of chemical dealloying is still remains unexplored. Furthermore, the $Fe_{73.5}Si_{13.5}B_9Cu_1Nb_3$ MGs in this work present a void channels-like architecture while the amorphous nature is well maintained. The catalytic activity will be performed on monitoring the methylene blue (MB) degradation by the use of the chemically dealloyed MGs with different morphologies. The catalytic stability as well as corrosion resistance will also be investigated for comparing their overall catalytic performance.

2. Materials and methods

2.1. Material preparation

The MGs with a nominal atomic composition of $Fe_{73.5}Si_{13.5}B_9Cu_1Nb_3$ were fabricated by a reported melt-spinning method [46, 47]. Typically, the master alloys with a specific atomic composition were initially prepared by an arc-melting process through melting the high purity elemental pieces (higher than 99.9 wt.%) under a Ti-gettered argon atmosphere for 4 times. Then the prepared master alloys were further melted in a quartz tube and were ejected onto a rotating Cu wheel with a tangenetial speed of 30 m/s in an argon atmosphere. The melt-spun $Fe_{73.5}Si_{13.5}B_9Cu_1Nb_3$ ribbons were measured as 30 - 40 μm thickness and 5 mm wide, denoted as as-spun FeCu in this work. The as-spun FeCu ribbons were further treated by chemical dealloying method in the diluted H_2SO_4 solutions with various concentrations of 0.05, 0.1, 0.2, and 0.5 M at different time intervals of 0.5, 1, 2, 5, 10, 15 and 24 h, respectively. After dealloying treatment, the ribbon surface was further ultrasonicated and washed by Milli-Q water (18.2 MΩ·cm) with three times for the dye degradation experiments.

2.2. Material characterization

5

The surface morphology and amorphous structure of the prepared samples were characterized by the scanning electron microscope (SEM) (FEI Verios 460), transmission electron microscopy (TEM) (JEOL JEM-2100) and X-ray diffraction (XRD) with *Co-Kα* radiation (PANalytical Empyrean, Netherlands), respectively. The surface atomic distribution of the catalysts was measured by the X-ray photoelectron spectroscopy (XPS) on a Kratos AXIS Ultra DLD instrument with *Al-Kα* X-ray and energy-dispersive X-ray spectroscopy (EDS) equipped on the SEM (FEI Verios 460). A differential scanning calorimeter (DSC) (Netzsch DSC-404C) with a heating rate of 20 ℃/min was employed to examine the thermal behavior of the samples. A Parstat 2273 electrochemical station with a traditional three-electrode cell was used for measuring the corrosion resistance of the samples. The prepared samples were used as the working electrode by connecting to a Luggin capillary bridge. A platinum sheet and a saturated calomel electrode (SCE) were employed as the counter electrode and the reference electrode, respectively. A simulated H_2SO_4 solution with a pH = 3.4 was chosen for the electrochemical measurements of the prepared glassy ribbons due to the initial pH 3.4 of dye solution after adding PMS. A pH meter (Oakton PC 2700 Benchtop Meter) was used to measure the pH values. The scanning rate was set as 1.0 mV/s. The scanning potential was started from -0.25 V to +1.0 V for the measurement of potentiodynamic polarization curves. In this electrochemical measurement, the potentials were recorded against SCE.

2.3. Catalytic activity

In catalytic tests, 50 mg (0.5 g/L) of the prepared catalysts was dispersed in a 100 ml of methylene blue (MB) solution with 20 ppm concentration (20 mg/L). Afterwards, 1.0 mM

6

peroxymonosulfate (PMS) was added into the dye solution for recording the catalytic experiment start. The dye solution was vibrated by a Vortex-Genie 2 mixer (Scientific Industries, Inc. USA) under a 300 W simulated solar light (Perfectlight Scientific Pty Ltd, Beijing, China) throughout the whole catalytic progress. The irradiation intensity was measured in the range of 7.7 - 14.8 $\mu W/cm^2$ by Newport optical power meter. All these mentioned operating variables for PMS activation were based on our previous reports [11, 17]. The water samples were taken out at predetermined time intervals of 1, 2, 5, 10, 15, 20, 25, 30, 40, 50 and 60 min, respectively, after which the sampled dye solutions were examined in turn by a UV-Vis spectrometer (Shelton, CT, USA). For total organic carbon (TOC) (TOC-VCSH, Shimadzu, Japan) and metal leaching (Optima 8300 ICP-OES Spectrometer, PerkinElmer) experiments, the sampled dye solutions were diluted 10 times by 2% w/w nitric acid (HNO_3) and treated by sodium nitrite ($NaNO_2$) with the same concentration of PMS to prevent further catalytic reaction. The maximum light absorbance (λ_{max}) of MB was recorded as 664 nm. The catalytic efficiency and reaction rate (k_{obs}) were calculated by Eqs. (1) and (2):

$$X = (C_0 - C)/C_0 \times 100\% \tag{1}$$

whereas C_0 and C are the initial concentration and the concentration at time t of MB dye, respectively.

$$ln(C_0/C) = k_{obs}\,t \tag{2}$$

whereas k_{obs} is the kinetic rate constant; C_0 is the original concentration of dye; C is the dye concentration at time t.

3. Results and discussion

3.1. Structures and chemical states

7

Figs. 1a and b present the HRTEM image and corresponding SAED pattern of the as-spun FeCu MGs, demonstrating the designed MGs are in good amorphous state [48]. In order to further confirm the amorphous nature of the designed as-spun FeCu MGs, DSC result is shown in Fig. 1c. Notably, the MG catalysts present two distinct crystallization processes with exothermic peaks at ~550 and 680 °C as well as the onset temperature (T_x) locating at 530 °C. The surface atomic components of FeCu glassy ribbons are initially characterized by EDS analysis in Fig. 1d. As shown in Fig. 1d, the energies of Fe, Si, B, Cu, Nb and O elements exhibit strong intensities and there are no other signals can be observed on the as-spun FeCu ribbons. The corresponding atomic percentages of Fe, Si, B, Cu and Nb have a very close ratio to the nominal expected value of the $Fe_{73.5}Si_{13.5}B_9Cu_1Nb_3$ glassy ribbons. To further confirm the chemical states and atomic bonds on the as-spun FeCu glassy ribbons, the XPS study is conducted as shown in Fig. 2. Fig. 2a presents the overall range XPS spectra of the FeCu ribbons. It is noted that only Fe, Si, B, Cu and Nb can be observed except the oxygen and carbon peaks which are owing to the adsorption of the molecular oxygen and carbon dioxides in the air [49]. No other impurity is obtained. By calculating the integral areas of each atomic component (Fe: 79.3, Si: 10.9, B: 8.0, Cu: 0.9 and Nb: 0.9), it is confirmed that the atoms are well dispersed on the ribbon surface with the nominal value of $Fe_{73.5}Si_{13.5}B_9Cu_1Nb_3$. Fig. 2b shows the high resolution of Fe 2p for the as-spun FeCu glassy ribbons. The observed binding energies at 706.1, 710.1 and 714.2 eV can be ascribed as Fe^0, Fe^{2+} and Fe^{3+}, respectively, indicating the ribbon surface comprises of Fe-O, Fe-Si and iron hydroxides atomic clusters on the FeCu glassy ribbon surface [10]. For the Si 2p spectra in Fig. 2c, the binding energies located at 98.3 and 101.4 eV are attributed to Si^0 and Si-O,

8

respectively. In the B 1s spectra in Fig. 2d, the B^0 and B-O bonds with binding energies at 192.1 and 188.0 eV can be observed. As shown in Fig. 2e, the binding energies at 931.5 and 928.8 eV indicate the distribution of zero valent Cu and the formation of Cu hydroxides, respectively. Fig. 2f presents the atomic distribution of Nb on the FeCu ribbon surface. The peaks located at 202.4 and 206.5 eV can be ascribed as the Nb^0 and the formation of Nb oxides, respectively.
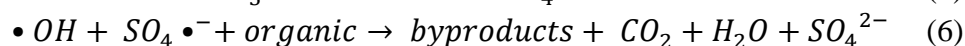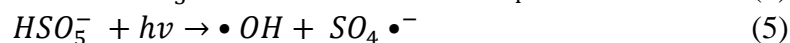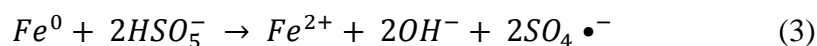
3.2. Surface morphologies

Improving surface roughness of the catalysts has been attracting particular attention to the potential applications and theoretical research due to their superior properties, such as large specific surface areas and enhanced adsorption ability to promote catalytic activities. Several reports have demonstrated that a crystallization behavior would occur during the chemical dealloying progress due to the atomic re-arrangement after one of the element leached, such as $Al_{85}Y_6Ni_6Co_3$ [41], $Fe_{76}Si_9B_{10}P_5$ [19] and $Mg_{65}Cu_{25}Y_{10}$ [26]. In comparison, the melt-spun FeCu glassy ribbons in this work still present a broad diffuse diffraction peak after being chemically treated for 2 – 15 h, as shown in XRD patterns in Fig. 3, indicating the dealloyed FeCu glassy ribbons are maintaining their amorphous nature [50-53]. Fig. 4 shows the variation of surface morphologies for the FeCu glassy ribbons at different dealloyed time in 0.05 M H_2SO_4 solution. It is noted that the free surface of the as-spun FeCu ribbons is ultra-smooth without any defects (Fig. 4a). After etching 2 – 5 h (Figs. 4 b and c), the metallic oxides are extensively expanded on the ribbon surface and continuously form several segments. After being treated for 10 h, the surface of FeCu glassy ribbons exhibits many dendritic void channels (Figs. 4 d and e) with large grains (Figs. 4 f and g). The selective dealloying of less active elements would generate an important volume shrinkage

to promote the final formation of interconnected voids [54]. Such surface morphology would significantly improve the surface roughness of the catalysts that might lead to a promoted catalytic activity. As shown in Fig. 4h, the Nb percentage is slightly increased compared with the as-spun FeCu ribbon, indicating that the atomic re-arrangement on the dealloyed ribbon surface is occurred during the chemical dealloying process. Furthermore, the results of XRD analysis in Fig. 3 demonstrate that the gradually produced Nb oxides on the ribbon surface are mainly in amorphous state. Such formation of Nb oxides on the ribbon surface with a strong stability and corrosion resistance would enhance the sustainability and reusability of the catalysts [11].

3.3. Catalytic activity

The catalytic activity of the as-prepared FeCu glassy ribbons toward MB color removal is conducted under the conditions of catalyst dosage: 0.5 g/L, irradiation intensity: 7.7 $\mu W/cm^2$, dye concentration: 20 ppm and PMS concentration: 1.0 mM. As shown in Fig. 5a, less than 10% of MB color removal could be achieved after 60 min without the addition of catalysts. Increasing the dealloying time from 0 h to 10 h for the FeCu ribbons could sharply enhance the MB degradation rate. For example, more than 90% of MB color removal can be achieved by the dealloyed 10 h FeCu ribbons at 40 min compared with only 60% efficiency of as-spun FeCu ribbons within the same time. The corresponding reaction rate increases from k_{obs} = 0.021 min^{-1} of as-spun ribbon to k_{obs} = 0.064 min^{-1} of dealloyed 10 h ribbon (Fig. 5b). Such improvement of the catalytic performance is attributed to the large surface roughness and void channels presents a significant enhancement for MB degradation compared with the as-spun FeCu ribbons. However, further increasing the dealloying time from 10 h to 24 h would sharply decrease the MB degradation efficiency, which is owing to the strong

10

extension of Nb oxides layer to impede the catalytic reaction between dye molecules and active sites in the catalysts [11]. Fig. 5c shows the UV-Vis spectra of MB color removal using 0.5 g/L of dealloyed 10 h FeCu glassy ribbons at various time intervals. The maximum adsorption peaks at $\lambda = 292$ nm and $\lambda = 664$ nm are characterized as the triazine group and heteropoly aromatic linkage for the MB dye. It can be seen that the peak at $\lambda = 664$ nm in the visible light region is completely invisible after being treated 40 min, reflecting the chromophore containing organic bonds are totally decomposed. The visible color change is shown in Fig. 5c inset. In addition, the peak at $\lambda = 292$ nm relating to the triazine group in the UV region is also gradually decreased from 0 min to 40 min, indicating the aromatic organic components in the dye are also decomposed [10]. The variation of H_2SO_4 concentration ranging from 0.05 M to 0.5 M at the treating time of 10 h on FeCu glassy ribbons is also conducted to verify the optimal dye degradation efficiency in Figs. 5 d and e. The result shows that the 0.05 M H_2SO_4 concentration presents the highest degradation efficiency with a reaction rate of $k_{obs} = 0.064$ min^{-1} for MB dye degradation (Fig. 5e). Therefore, 0.05 M H_2SO_4 concentration is selected for the following catalytic investigations. The chemical reactions between the $Fe_{73.5}Si_{13.5}B_9Cu_1Nb_3$ metallic glass and PMS are presented in Eqs. 3-6 below.

$$Fe^0 + 2HSO_5^- \rightarrow Fe^{2+} + 2OH^- + 2SO_4 \bullet^- \qquad (3)$$
$$Fe^{2+} + HSO_5^- \rightarrow Fe^{3+} + OH^- + SO_4 \bullet^- \qquad (4)$$
$$HSO_5^- + hv \rightarrow \bullet OH + SO_4 \bullet^- \qquad (5)$$
$$\bullet OH + SO_4 \bullet^- + organic \rightarrow byproducts + CO_2 + H_2O + SO_4^{2-} \qquad (6)$$

To demonstrate the organic matters are oxidized to CO_2 and H_2O, the comparable TOC results are conducted for the as-prepared samples in Fig. 6. It is noted that the TOC removal rate sharply improves from 38% of as-spun FeCu ribbon to 50% of dealloyed 10 h FeCu

ribbon within 30 min, presenting the significance of the facile chemical dealloying for the glassy ribbons. The metal leaching effect is also important to be investigated in wastewater treatment due to large metal sludge would cause severe secondary pollution. As shown in Fig. 6, the Fe concentration of the as-spun FeCu ribbons reach to 0.40 mg/L at 30 min, whereas only less than 0.15 mg/L of Fe is observed for the dealloyed FeCu ribbons. The FeCu glassy ribbons have a negligible Fe leaching that is much lower than the European Union standard of 2 mg/L, owing to the micro-alloying of Nb atomic configurations in the FeCu glassy ribbons. This slight leaching of Fe (ferrous or ferric) ions from the FeCu ribbons would also assist the PMS activation to produce hydroxyl radicals ($\bullet$OH) and sulfate radicals (SO$_4\bullet^-$) in dye degradation [37].

3.4. Catalytic stability

Considering overall catalytic performance, the catalytic stability of a catalyst is also very important to be investigated in the practical applications. Fig. 7 shows the catalytic reusability of the dealloyed 10 h FeCu glassy ribbons. As shown in Fig. 7, the dealloyed 10 h FeCu glassy ribbons can be reused up to 25 times without significantly loosing catalytic efficiency. The micro-alloying of Cu (1%) and Nb (3%) atoms into the FeSiB glassy ribbon could largely improve the surface stability that plays a significant role during the chemical dealloying progress. However, a sharp decrease of dye degradation efficiency is observed after being reused for 30 times for the dealloyed 10 h FeCu glassy ribbons. As shown in Fig. 8, the surface morphology of dendritic void channels for the dealloyed 10 h FeCu ribbons (Figs. 4 d-g) is completely changed to many densely packed segments. According to elemental mapping observation in Fig. 8b, the atomic distributions of the segments are mainly Nb, O and S, indicating the Nb oxides with a strong stability is precipitated on the

ribbon surface. The contacted area of Fe and PMS is continuously reduced to finally cause the decrease of dye degradation efficiency. The slight adsorption of S element on the surface is originated from the MB dye and PMS molecules. It is well accepted that the stability of a catalyst has a strong relationship with their corrosion resistance. Fig. 9 presents the potentiodynamic polarization curves of the as-spun and dealloyed ribbons after the open circuit potential (OCP) stabilization. It is observed that all the glassy ribbons could achieve large potential values of 1.0 V_{SCE} without reaching breakdown potential, demonstrating the strong corrosion resistance of the Fe-based glassy ribbons [55]. In addition, although all the glassy ribbons present similar anodic polarisation behaviors, the dealloyed 10 h FeCu ribbon with a higher potential value of $-$ 0.35 V_{SCE} demonstrates stronger corrosion resistance than other counterparts. This result indicates that the dealloyed 10 h FeCu ribbons are more qualified under complex environment of industrial wastewater in the practical application.

4. Conclusion

In this work, we develop a non-noble and multicomponent chemically dealloyed $Fe_{73.5}Si_{13.5}B_9Cu_1Nb_3$ metallic glass catalyst that presents a fascinating catalytic efficiency while maintaining a remarkable stability for wastewater remediation. The chemically dealloyed $Fe_{73.5}Si_{13.5}B_9Cu_1Nb_3$ metallic glass with a void channel-like structure presented a significant improvement on surface roughness in catalytic application. The micro-alloying of Cu and Nb elements could give rise to form strong Nb oxide protective layer, leading to a large surface area and a promoted surface roughness by chemical dealloying for dye degradation. The dealloyed 10 h $Fe_{73.5}Si_{13.5}B_9Cu_1Nb_3$ glassy ribbons presented 3 times higher dye degradation efficiency than the as-spun counterparts and could be reused up to 25

times without loosing catalytic efficiency, demonstrating a great potential in pracical applications. In addition, the corrosion resistance of the chemically dealloyed $Fe_{73.5}Si_{13.5}B_9Cu_1Nb_3$ catalysts was also significantly promoted compared to the as-spun ribbons, showing a compelling self-stability in the dye containing water environment. The presented results in this work reveal a new method to improve the overall catalytic activity and provide new opportunities into the design of novel metallic catalysts.

Acknowledgements

Conflicts of interest

The authors declare no conflict of interest.

References

[1] S.X. Liang, Z. Jia, Y.J. Liu, W.C. Zhang, W.M. Wang, J. Lu, L.-C. Zhang, Compelling Rejuvenated Catalytic Performance in Metallic Glasses, Adv. Mater. 30 (2018) 1802764.

[2] L.-C. Zhang, S.-X. Liang, Recent Advances of Fe-based Metallic Glasses in Functional Catalytic Applications, Chem. Asian J. 13 (2018) 3575-3592.

[3] Y. Pei, G. Zhou, N. Luan, B. Zong, M. Qiao, F. Tao, Synthesis and catalysis of chemically reduced metal–metalloid amorphous alloys, Chem. Soc. Rev. 41 (2012) 8140-8162.

[4] H. Li, H. Li, W. Dai, M. Qiao, Preparation of the Ni-B amorphous alloys with variable boron content and its correlation to the hydrogenation activity, Appl. Catal. A: Gen. 238 (2003) 119-130.

[5] S. Wang, W. Wei, Y. Zhao, H. Li, H. Li, Ru–B amorphous alloy deposited on mesoporous silica nanospheres: An efficient catalyst for d-glucose hydrogenation to d-sorbitol, Catal. Today 258 (2015) 327-336.

[6] J.Q. Wang, Y.H. Liu, M.W. Chen, G.Q. Xie, D.V. Louzguine-Luzgin, A. Inoue, J.H. Perepezko, Rapid Degradation of Azo Dye by Fe-Based Metallic Glass Powder, Adv. Funct. Mater. 22 (2012) 2567-2570.

[7] J.-Q. Wang, Y.-H. Liu, M.-W. Chen, D.V. Louzguine-Luzgin, A. Inoue, J.H. Perepezko, Excellent capability in degrading azo dyes by MgZn-based metallic glass powders, Sci. Rep. 2 (2012) 418.

[8] H. Li, W. Wei, Y. Zhao, H. Li, Preparation and catalytic applications of amorphous alloys, in: Catalysis, The Royal Society of Chemistry, 2015, pp. 144-186.

[9] L. Xu, W. Wei, H. Li, H. Li, Combination of Enzyme and Ru–B Amorphous Alloy Encapsulated in Yolk-Shell Silica for One-Pot Dextrin Conversion to Sorbitol, ACS Catal. 4 (2014) 251-258.

[10] Z. Jia, X. Duan, P. Qin, W. C. Zhang, W. M. Wang, C. Yang, H. Sun, S. Wang, L.C. Zhang, Disordered Atomic Packing Structure of Metallic Glass: Toward Ultrafast Hydroxyl Radicals Production Rate and Strong Electron Transfer Ability in Catalytic Performance, Adv. Funct. Mater. 27 (2017) 1702258.

[11] Z. Jia, J. Kang, W.C. Zhang, W.M. Wang, C. Yang, H. Sun, D. Habibi, L.C. Zhang, Surface aging behaviour of Fe-based amorphous alloys as catalysts during heterogeneous photo Fenton-like process for water treatment, Appl. Catal. B: Environ. 204 (2017) 537-547.

[12] Y. Tang, Y. Shao, N. Chen, X. Liu, S.Q. Chen, K.F. Yao, Insight into the high reactivity of commercial Fe-Si-B amorphous zero-valent iron in degrading azo dye solutions, RSC Adv. 5 (2015) 34032-34039.

[13] X. Wang, Y. Pan, Z. Zhu, J. Wu, Efficient degradation of rhodamine B using Fe-based metallic glass catalyst by Fenton-like process, Chemosphere 117 (2014) 638-643.

[14] J. Yang, X. Bian, Y. Bai, X. Lv, P. Wang, Rapid organism degradation function of Fe-based alloys in high concentration wastewater, J. Non-Cryst. Solids. 358 (2012) 2571-2574.

[15] P. Wang, X. Bian, Y. Li, Catalytic oxidation of phenol in wastewater — A new application of the amorphous Fe78Si9B13 alloy, Chin. Sci. Bull. 57 (2012) 33-40.

[16] C. Zhang, Z. Zhu, H. Zhang, Z. Hu, Rapid decolorization of Acid Orange II aqueous solution by amorphous zero-valent iron, J. Environ. Sci. 24 (2012) 1021-1026.

[17] J.C. Wang, Z. Jia, S.X. Liang, P. Qin, W.C. Zhang, W.M. Wang, T.B. Sercombe, L.C. Zhang, Fe73.5Si13.5B9Cu1Nb3 metallic glass: Rapid activation of peroxymonosulfate towards ultrafast Eosin Y degradation, Mater. Des. 140 (2018) 73-84.

[18] Y. Tang, Y. Shao, N. Chen, K.-F. Yao, Rapid decomposition of Direct Blue 6 in neutral solution by Fe-B amorphous alloys, RSC Adv. 5 (2015) 6215-6221.

[19] N. Weng, F. Wang, F. Qin, W. Tang, Z. Dan, Enhanced Azo-Dyes Degradation Performance of Fe-Si-B-P Nanoporous Architecture, Materials 10 (2017) 1001.

[20] X.-F. Li, S.-X. Liang, X.-W. Xi, Z. Jia, S.-K. Xie, H.-C. Lin, J.-P. Hu, L.-C. Zhang, Excellent Performance

of Fe78Si9B13 Metallic Glass for Activating Peroxymonosulfate in Degradation of Naphthol Green B, Metals 7 (2017) 273.

[21] Z. Jia, S.X. Liang, W.C. Zhang, W.M. Wang, C. Yang, L.C. Zhang, Heterogeneous photo Fenton-like degradation of the cibacron brilliant red 3B-A dye using amorphous Fe78Si9B13 and Fe73.5Si13.5B9Cu1Nb3 alloys: The influence of adsorption, J. Taiwan Inst. Chem. Eng. 71 (2017) 128-136.

[22] S.X. Liang, Z. Jia, W.C. Zhang, W.M. Wang, L.C. Zhang, Rapid malachite green degradation using Fe73.5Si13.5B9Cu1Nb3 metallic glass for activation of persulfate under UV-Vis light, Mater. Des. 119 (2017) 244-253.

[23] S. Chen, G. Yang, S. Luo, S. Yin, J. Jia, Z. Li, S. Gao, Y. Shao, K. Yao, Unexpected high performance of Fe-based nanocrystallized ribbons for azo dye decomposition, J. Mater. Chem. A 5 (2017) 14230-14240.

[24] S. Chen, N. Chen, M. Cheng, S. Luo, Y. Shao, K. Yao, Multi-phase nanocrystallization induced fast degradation of methyl orange by annealing Fe-based amorphous ribbons, Intermetallics 90 (2017) 30-35.

[25] C. Zhang, Z. Zhu, H. Zhang, Mg-based amorphous alloys for decolorization of azo dyes, Res. Phys. 7 (2017) 2054-2056.

[26] X. Luo, R. Li, J. Zong, Y. Zhang, H. Li, T. Zhang, Enhanced degradation of azo dye by nanoporous-copper-decorated Mg–Cu–Y metallic glass powder through dealloying pretreatment, Appl. Surf. Sci. 305 (2014) 314-320.

[27] P. Chen, X. Hu, Y. Qi, X. Wang, Z. Li, L. Zhao, S. Liu, C. Cui, Rapid Degradation of Azo Dyes by Melt-Spun Mg-Zn-Ca Metallic Glass in Artificial Seawater, Metals 7 (2017) 485.

[28] M. Ramya, M. Karthika, R. Selvakumar, B. Raj, K.R. Ravi, A facile and efficient single step ball milling process for synthesis of partially amorphous Mg-Zn-Ca alloy powders for dye degradation, J. Alloys Compd. 696 (2017) 185-192.

[29] M. Iqbal, W.H. Wang, Synthesis and characterization of Mg-based amorphous alloys and their use for decolorization of Azo dyes, IOP Conf. Ser. Mater. Sci. Eng. 60 (2014) 012035.

[30] Y.F. Zhao, J.J. Si, J.G. Song, Q. Yang, X.D. Hui, Synthesis of Mg–Zn–Ca metallic glasses by gas-atomization and their excellent capability in degrading azo dyes, Mater. Sci. Eng. B 181 (2014) 46-55.

[31] S. Das, S. Garrison, S. Mukherjee, Bi-Functional Mechanism in Degradation of Toxic Water Pollutants by Catalytic Amorphous Metals, Adv. Eng. Mater. 18 (2016) 214-218.

[32] P. Wang, J.-Q. Wang, H. Li, H. Yang, J. Huo, J. Wang, C. Chang, X. Wang, R.-W. Li, G. Wang, Fast decolorization of azo dyes in both alkaline and acidic solutions by Al-based metallic glasses, J. Alloys Compd. 701 (2017) 759-767.

[33] X.D. Qin, Z.W. Zhu, G. Liu, H.M. Fu, H.W. Zhang, A.M. Wang, H. Li, H.F. Zhang, Ultrafast degradation of azo dyes catalyzed by cobalt-based metallic glass, Sci. Rep. 5 (2015) 18226.

[34] C. Zhang, Q. Sun, K. Liu, From adsorption to reductive degradation: Different decolorization properties of metallic glasses based on different iron-group elements, J. Alloys Compd. 741 (2018) 1040-1047.

[35] Z. Jia, L. B. T. La, W.C. Zhang, S.X. Liang, B. Jiang, S.K. Xie, D. Habibi, L.C. Zhang., Strong enhancement on dye photocatalytic degradation by ball-milling TiO2: a study of cationic and anionic dyes, J. Mater. Sci. Technol. 33 (2017) 856-863.

[36] Z. Jia, W.C. Zhang, W.M. Wang, D. Habibi, L.C. Zhang, Amorphous Fe78Si9B13 alloy: An efficient and reusable photo-enhanced Fenton-like catalyst in degradation of cibacron brilliant red 3B-A dye under UV–vis light, Appl. Catal. B: Environ. 192 (2016) 46-56.

[37] Z. Jia, X. Duan, W.C. Zhang, W.M. Wang, H. Sun, S. Wang, C. Yang, L.C. Zhang., Ultra-sustainable Fe78Si9B13 metallic glass as a catalyst for activation of persulfate on methylene blue degradation under UV-Vis light, Sci. Rep. 6 (2016) 38520.

[38] Z. Jia, J.C. Wang, S.X. Liang, W.C. Zhang, W.M. Wang, L.C. Zhang, Activation of peroxymonosulfate by Fe78Si9B13 metallic glass: the influence of crystallization J. Alloys Compd. 728 (2017) 525-533.

[39] S.X. Liang, Z. Jia, W.C. Zhang, X.F. Li, W.M. Wang, H.C. Lin, L.C. Zhang, Ultrafast activation efficiency of three peroxides by Fe78Si9B13 metallic glass under photo-enhanced oxidative degradation: a comparative study, Appl. Catal. B: Environ. 221 (2018) 108-118.

[40] Z. Deng, X.H. Zhang, K.C. Chan, L. Liu, T. Li, Fe-based metallic glass catalyst with nanoporous surface for azo dye degradation, Chemosphere 174 (2017) 76-81.

[41] H.J. Qiu, J.Q. Wang, P. Liu, Y. Wang, M.W. Chen, Hierarchical nanoporous metal/metal-oxide composite by dealloying metallic glass for high-performance energy storage, Corros. Sci. 96 (2015) 196-202.

[42] W. Xu, S. Zhu, Y. Liang, Z. Cui, X. Yang, A. Inoue, H. Wang, A highly efficient electrocatalyst based on amorphous Pd-Cu-S material for hydrogen evolution reaction, J. Mater. Chem. A 5 (2017) 18793-18800.

[43] W.H. Wang, J.J. Lewandowski, A.L. Greer, Understanding the Glass-forming Ability of Cu50Zr50 Alloys in Terms of a Metastable Eutectic, J. Mater. Res. 20 (2005) 2307-2313.

[44] W.H. Wang, Roles of minor additions in formation and properties of bulk metallic glasses, Prog. Mater. Sci. 52 (2007) 540-596.

[45] H.-B. Yu, W.-H. Wang, K. Samwer, The β relaxation in metallic glasses: an overview, Mater. Today 16 (2013) 183-191.

[46] L.C. Zhang, J. Xu, Glass-forming ability of melt-spun multicomponent (Ti, Zr, Hf)–(Cu, Ni, Co)–Al alloys with equiatomic substitution, J. Non-Cryst. Solids 347 (2004) 166-172.

[47] H.B. Lu, L.C. Zhang, A. Gebert, L. Schultz, Pitting corrosion of Cu–Zr metallic glasses in hydrochloric acid solutions, J. Alloys Compd. 462 (2008) 60-67.

[48] L.C. Zhang, J. Xu, E. Ma, Mechanically Alloyed Amorphous Ti50(Cu0.45Ni0.55)44–xAlxSi4B2 Alloys with Supercooled Liquid Region, J. Mater. Res. 17 (2002) 1743-1749.

[49] F. Hu, S. Zhu, S. Chen, Y. Li, L. Ma, T. Wu, Y. Zhang, C. Wang, C. Liu, X. Yang, L. Song, X. Yang, Y. Xiong, Amorphous Metallic NiFeP: A Conductive Bulk Material Achieving High Activity for Oxygen Evolution Reaction in Both Alkaline and Acidic Media, Adv. Mater. 29 (2017) 1606570.

[50] P. Yu, L.C. Zhang, W.Y. Zhang, J. Das, K.B. Kim, J. Eckert, Interfacial reaction during the fabrication of Ni60Nb40 metallic glass particles-reinforced Al based MMCs, Mater. Sci. Eng. A 444 (2007) 206-213.

[51] M. Calin, L.C. Zhang, J. Eckert, Tailoring of microstructure and mechanical properties of a Ti-based bulk metallic glass-forming alloy, Scr. Mater. 57 (2007) 1101-1104.

[52] L.C. Zhang, K.B. Kim, P. Yu, W.Y. Zhang, U. Kunz, J. Eckert, Amorphization in mechanically alloyed (Ti, Zr, Nb)–(Cu, Ni)–Al equiatomic alloys, J. Alloys Compd. 428 (2007) 157-163.

[53] L.C. Zhang, Z.Q. Shen, J. Xu, Mechanically milling-induced amorphization in Sn-containing Ti-based multicomponent alloy systems, Mater. Sci. Eng. A 394 (2005) 204-209.

[54] H.J. Qiu, X. Shen, J.Q. Wang, A. Hirata, T. Fujita, Y. Wang, M.W. Chen, Aligned Nanoporous Pt–Cu Bimetallic Microwires with High Catalytic Activity toward Methanol Electrooxidation, ACS Catal. 5 (2015) 3779-3785.

[55] S.D. Zhang, W.L. Zhang, S.G. Wang, X.J. Gu, J.Q. Wang, Characterisation of three-dimensional porosity in an Fe-based amorphous coating and its correlation with corrosion behaviour, Corros. Sci. 93 (2015) 211-221.

Figure captions

Figure 1 (a) HRTEM image, (b) SAED pattern, (c) DSC and (d) EDS results of the as-spun $Fe_{73.5}Si_{13.5}B_9Cu_1Nb_3$ metallic glasses

Figure 2 (a) Full range and high resolution XPS spectra of (b) Fe 2p, (c) Si 2p, (d) B 1S, (e) Cu 2p and (f) Nb 3d for the as-spun $Fe_{73.5}Si_{13.5}B_9Cu_1Nb_3$ metallic glasses

Figure 3 XRD patterns of the as-spun and chemically dealloyed (0.05 M H_2SO_4) $Fe_{73.5}Si_{13.5}B_9Cu_1Nb_3$ metallic glasses

Figure 4 SEM images of (a) as-spun, (b) dealloyed 2h, (c) dealloyed 5h and (d) dealloyed 10h $Fe_{73.5}Si_{13.5}B_9Cu_1Nb_3$ metallic glasses and (e-g) selected areas of the dealloyed 10h $Fe_{73.5}Si_{13.5}B_9Cu_1Nb_3$ ribbon in 0.05M H_2SO_4 solution, h) EDS result of dealloyed 10h $Fe_{73.5}Si_{13.5}B_9Cu_1Nb_3$ ribbon

Figure 5 (a) MB color removals and (b) the corresponding kinetic rates (k_{obs}) by $Fe_{73.5}Si_{13.5}B_9Cu_1Nb_3$ metallic glasses at different dealloying time, (c) UV-Vis spectra of MB degradation in the presence of the dealloyed 10 h $Fe_{73.5}Si_{13.5}B_9Cu_1Nb_3$ metallic glasses (inset is the "big picture" of visible color change, experimental conditions comprising of 0.5 g/L of catalyst, 7.7 µW/cm^2 of light intensity, 20 ppm of MB dye, 1.0 mM of PMS and room temperature), (d) MB color removals and (e) reaction rates (k_{obs}) by dealloyed $Fe_{73.5}Si_{13.5}B_9Cu_1Nb_3$ glassy ribbon at different H_2SO_4 concentrations at treated time of 10 h

Figure 6 TOC removals and Fe leaching concentrations of as-spun and dealloyed 10 h $Fe_{73.5}Si_{13.5}B_9Cu_1Nb_3$ metallic glasses

Figure 7 Reusability of the dealloyed $Fe_{73.5}Si_{13.5}B_9Cu_1Nb_3$ metallic glasses (catalyst dosage: 0.5 g/L, light intensity: 7.7 µW/cm^2, dye concentration: 20 ppm and PMS concentration: 1.0 mM)

Figure 8 SEM image of the 30th run of dealloyed 10 h $Fe_{73.5}Si_{13.5}B_9Cu_1Nb_3$ metallic glasses and (b) corresponding elemental mapping analysis on ribbon surface

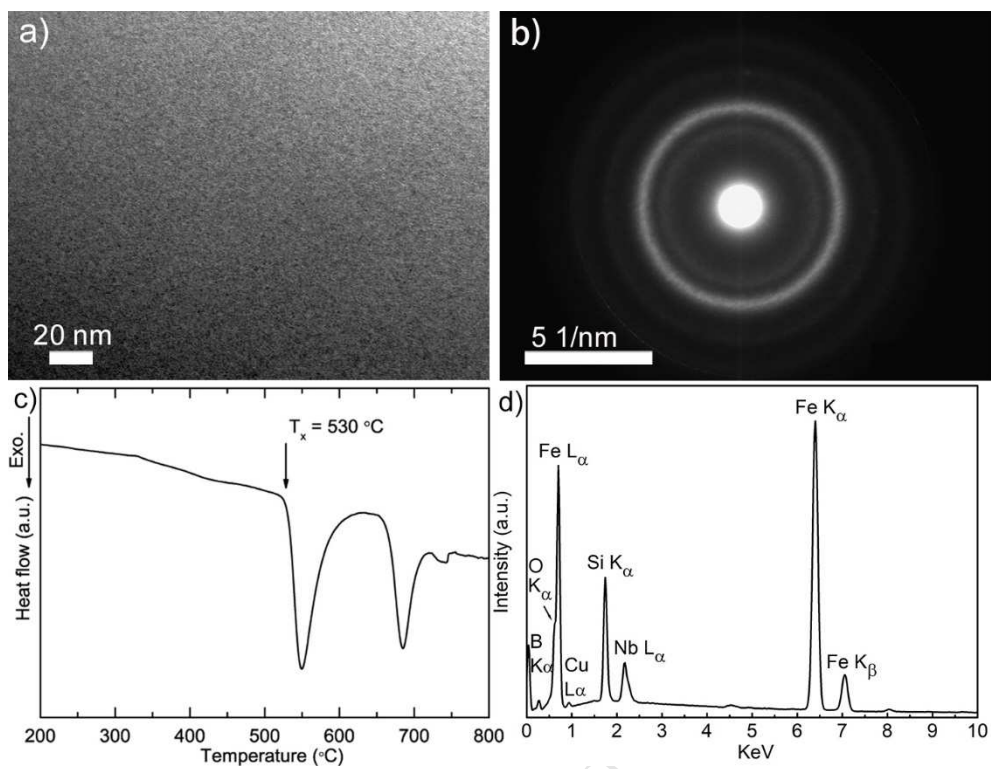**Figure 9** Potentiodynamic polarization curves for the as-prepared catalysts
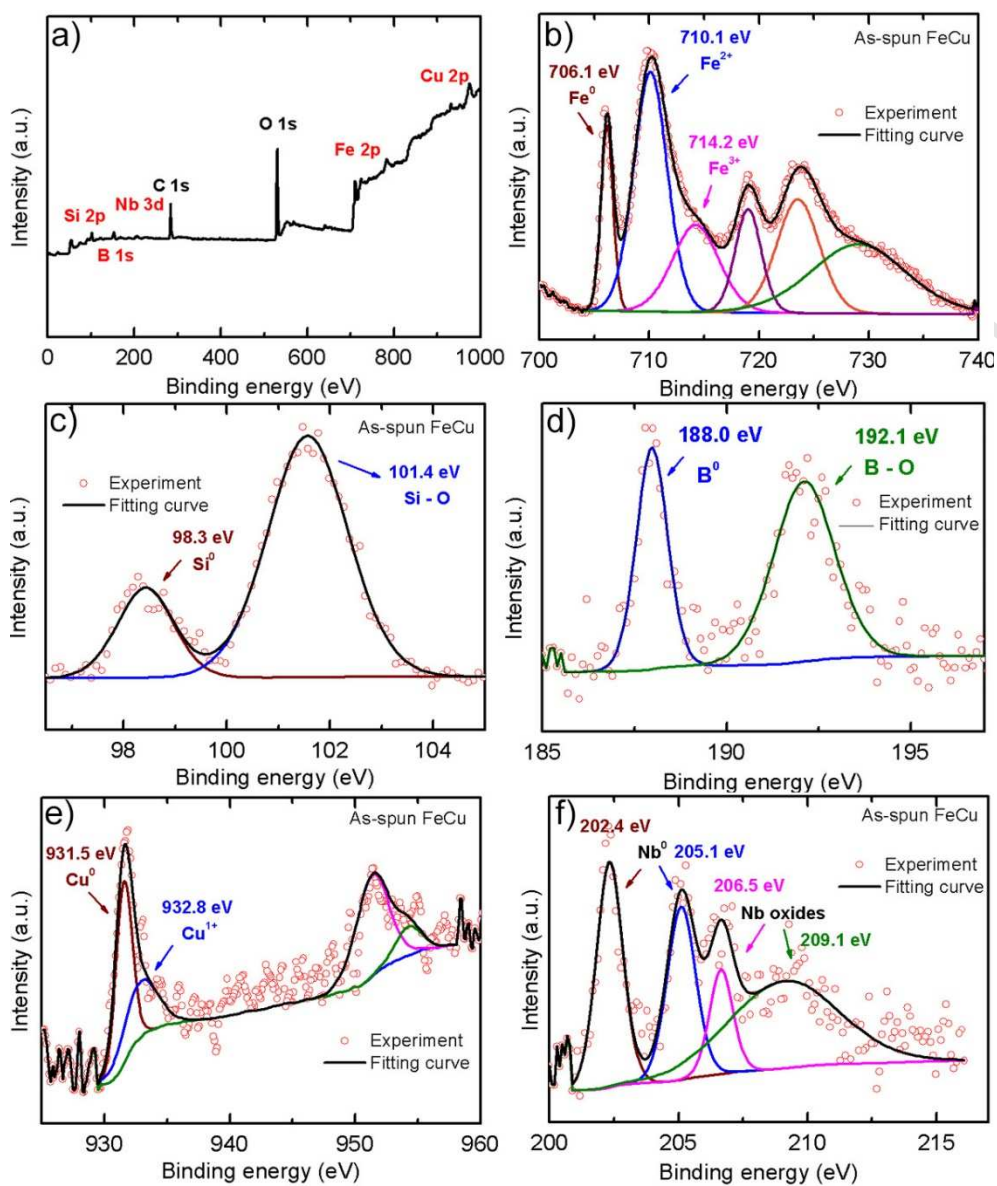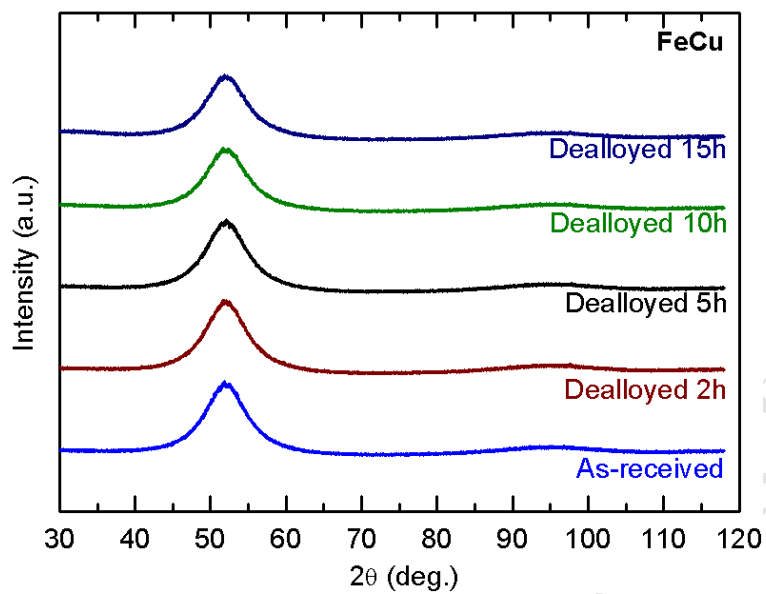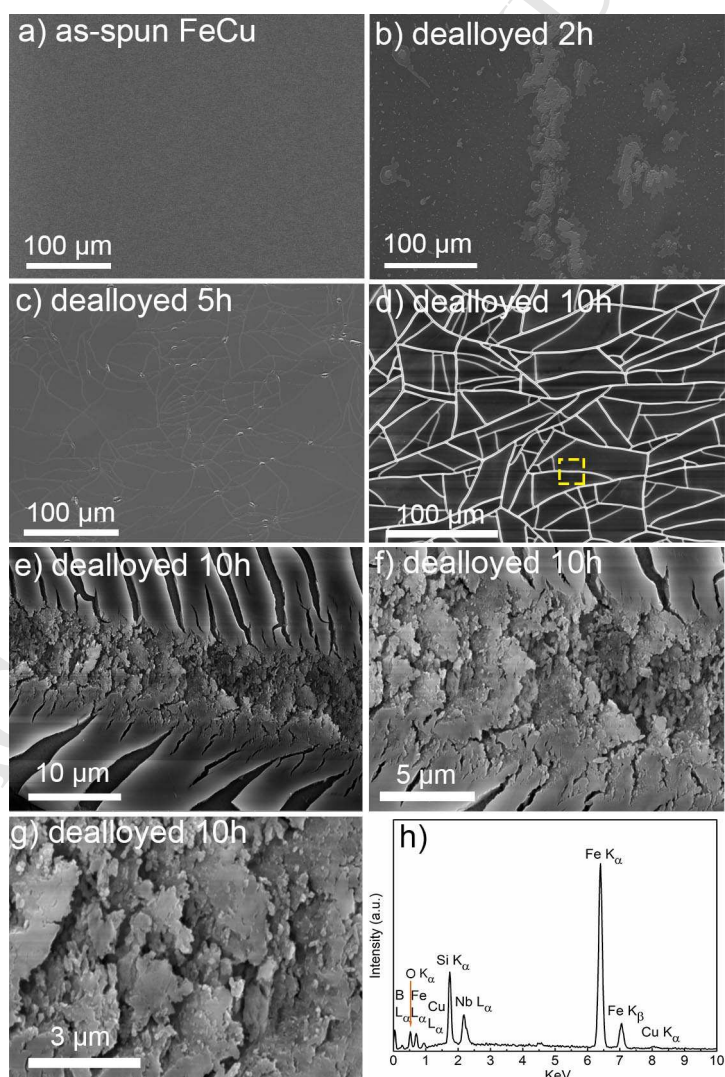
Figure 1

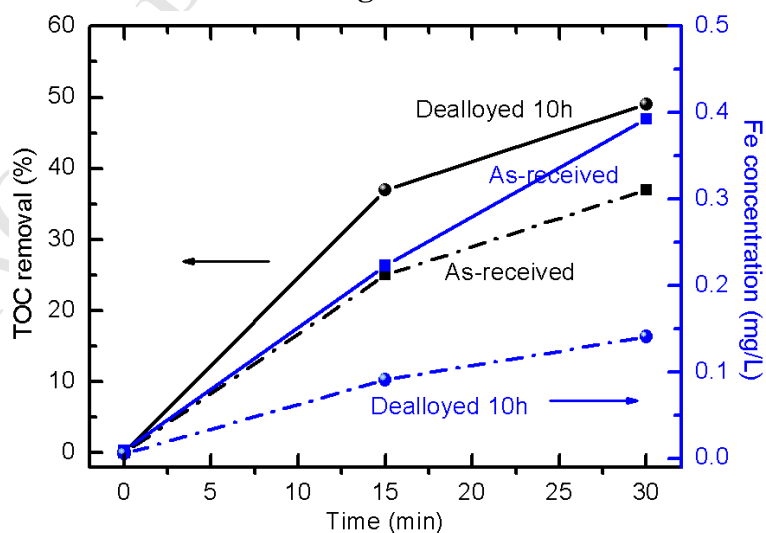**Figure 2**

Figure 3

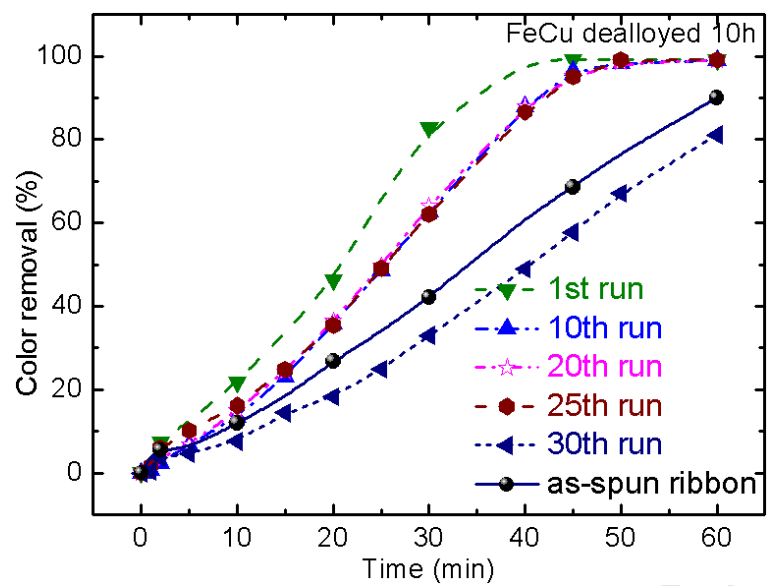**Figure 4**
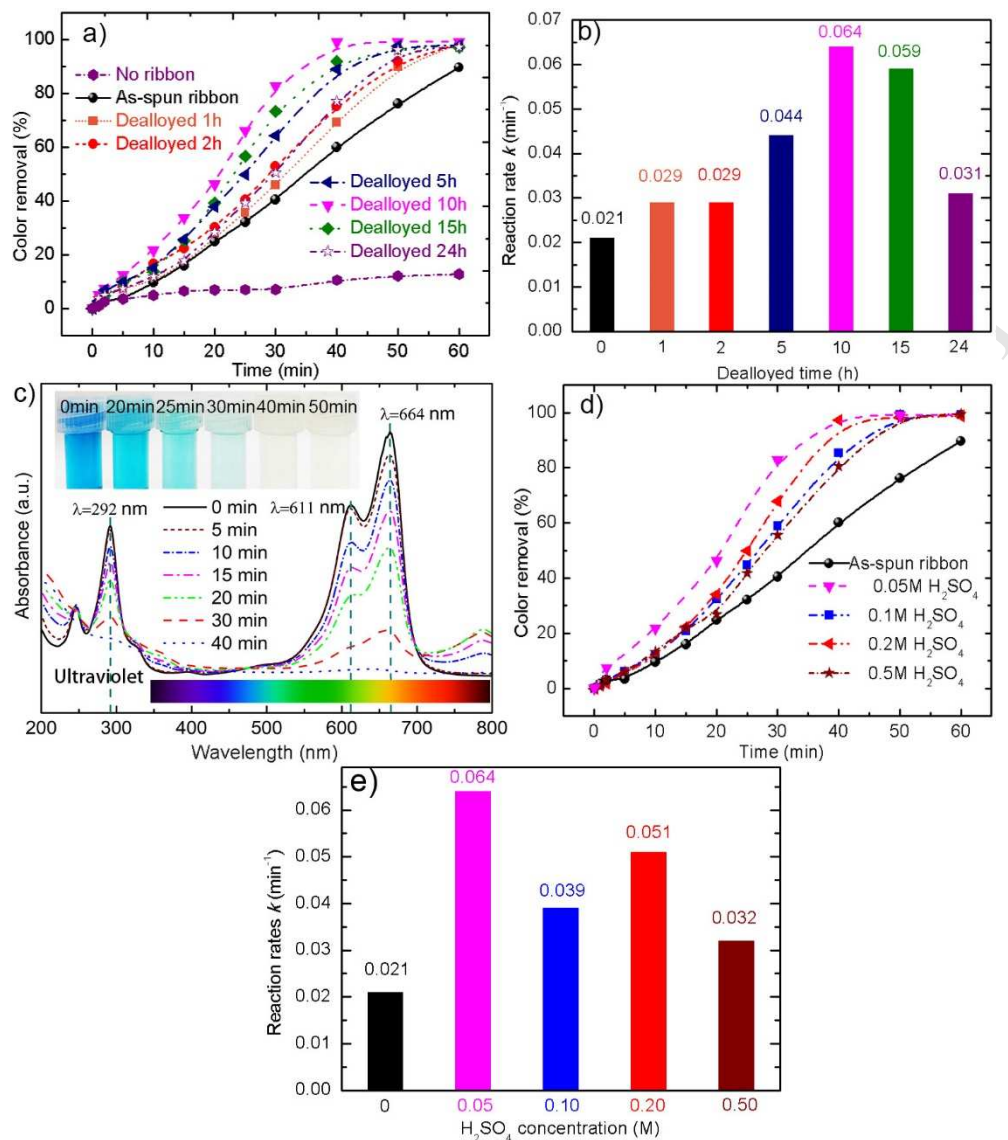
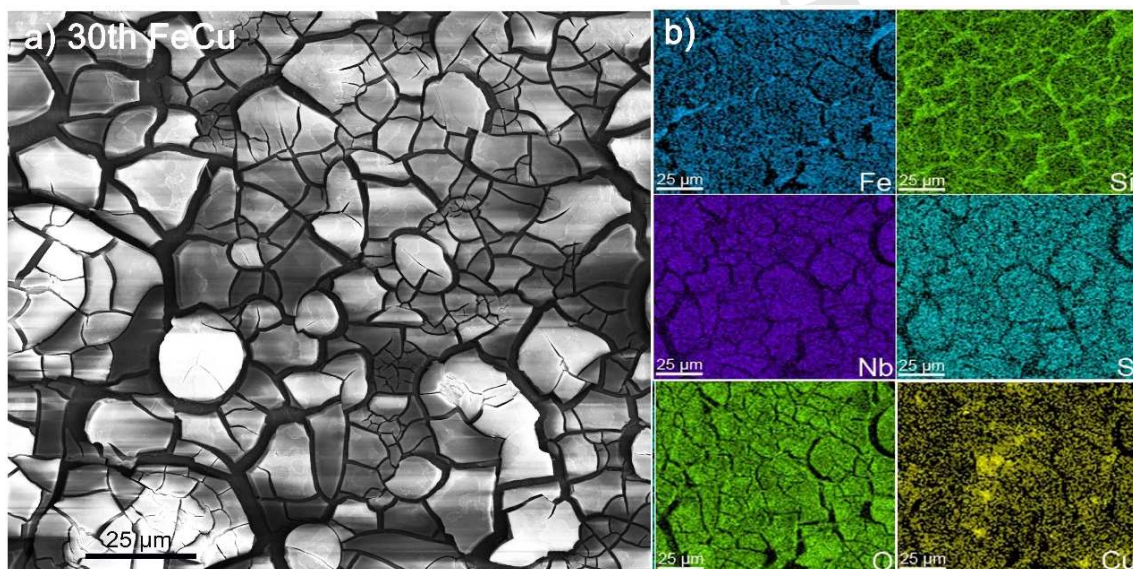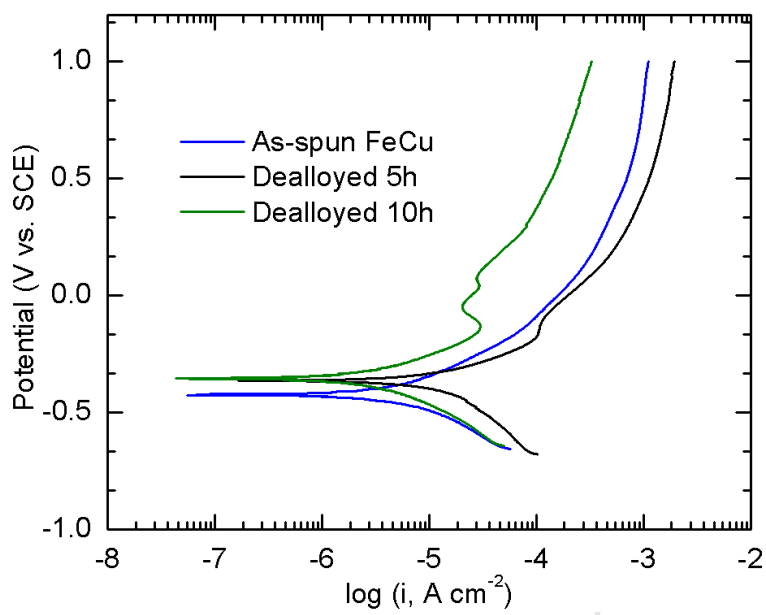**Figure 5**

Figure 6

Figure 7

Figure 8

Figure 9

Highlights

- A void channels-like structured melt-spun metallic glass is reported

- Dealloyed metallic glasses show 3 times higher reaction rate than counterparts

- Dealloyed $Fe_{73.5}Si_{13.5}B_9Cu_1Nb_3$ ribbons can be reused for 25 times

- A strong corrosion resistance in dealloyed $Fe_{73.5}Si_{13.5}B_9Cu_1Nb_3$ ribbons is studied